ChemPubSoc Europe

DOI: 10.1002/cphc.201600511

CHEMPHYSCHEM Articles

Engineering Chemically Exfoliated Large-Area Two-Dimensional MoS_2 Nanolayers with Porphyrins for Improved Light Harvesting

Hanyu Zhang,[a] Jungwook Choi,[b] Arjun Ramani,[a] Damien Voiry,[c] Sean N. Natoli,[d] Manish Chhowalla,[c] David R. McMillin,[d] and Jong Hyun Choi*[a]

Molybdenum disulfide (MoS_2) is a promising candidate for electronic and optoelectronic applications. However, its application in light harvesting has been limited in part due to crystal defects, often related to small crystallite sizes, which diminish charge separation and transfer. Here we demonstrate a surface-engineering strategy for 2D MoS_2 to improve its photoelectrochemical properties. Chemically exfoliated large-area MoS_2 thin films were interfaced with eight molecules from three porphyrin families: zinc(II)-, gallium(III)-, iron(III)-centered, and metal-free protoporphyrin IX (ZnPP, GaPP, FePP, H_2PP); metal-free and zinc(II) tetra-(*N*-methyl-4-pyridyl)porphyrin (H_2T4, ZnT4); and metal-free and zinc(II) tetraphenylporphyrin (H_2TPP, ZnTPP). We found that the photocurrents from MoS_2 films under visible-light illumination are strongly dependent on the interfacial molecules and that the photocurrent enhancement is closely correlated with the highest occupied molecular orbital (HOMO) levels of the porphyrins, which suppress the recombination of electron–hole pairs in the photoexcited MoS_2 films. A maximum tenfold increase was observed for MoS_2 functionalized with ZnPP compared with pristine MoS_2 films, whereas ZnT4-functionalized MoS_2 demonstrated small increases in photocurrent. The application of bias voltage on MoS_2 films can further promote photocurrent enhancements and control current directions. Our results suggest a facile route to render 2D MoS_2 films useful for potential high-performance light-harvesting applications.

1. Introduction

Layered transition-metal dichalcogenide (TMDC) materials have received much attention, due to the accessibility of atomically thin layers and unique layer-number-dependent physical properties.[1] For example, molybdenum disulfide (MoS_2) transitions from an indirect bandgap semiconductor in the bulk phase to a direct bandgap semiconductor as monolayer sheets, with strong photoluminescence (PL) centered at around 1.88 eV.[1a] This atomically thin semiconductor demonstrates a high in-plane carrier mobility and on/off ratio,[2] which are critical in nanoelectronics and optoelectronics.[1a,3]

MoS_2 also has been explored as a promising photoelectrode material in photoelectrochemical (PEC) cells.[4] Their good stability against photo-damage[4a] and wide range of visible absorption render MoS_2 useful as photoanodes.[5] Given the cost-effectiveness and excellent electrocatalytic properties of MoS_2, it has been explored as an additive agent for counter electrodes in dye-sensitized solar cells (DSSCs).[4d–f] An atomically thin layer of MoS_2 coated on the counter electrode considerably enhanced the overall performance of DSSCs.[4e] MoS_2 may also be exploited as a catalyst for the hydrogen-evolution reaction (HER),[6] in which sulfur vacancies from optimized 2H-MoS_2 monolayers can serve as catalytic sites.[6b]

Despite the advantages of MoS_2, there are several challenges in utilizing MoS_2 in PEC or other solar-energy harvesting applications. Large-area two-dimensional (2D) MoS_2 films are desirable, but their preparation is challenging. Chhowalla and coworkers addressed this issue recently, to considerable extent, by introducing Li-ion intercalation followed by forced hydration.[7] The exfoliated MoS_2 flakes in aqueous solution were then deposited on a membrane that was transferred to indium tin oxide (ITO)-coated glasses to form active working electrodes after appropriate thermal annealing.[4b,8] This approach shows the potential to create large-area 2D materials in a cost-effective manner.[9]

Although large-area fabrication is now possible, several other issues still remain to be addressed, such as nonradiative recombination and suppression of charge transfer due to the small crystallites and crystal defects.[4b,10] To overcome these

[a] H. Zhang, A. Ramani, Prof. J. H. Choi
School of Mechanical Engineering
Purdue University, West Lafayette
IN 47907 (USA)
E-mail: jchoi@purdue.edu

[b] Prof. J. Choi
School of Mechanical Engineering
Yeungnam University
Gyeongsan 38541 (Republic of Korea)

[c] Dr. D. Voiry, Prof. M. Chhowalla
Materials Science and Engineering
Rutgers University, Piscataway
NJ 08854 (USA)

[d] S. N. Natoli, Prof. D. R. McMillin
Department of Chemistry, Purdue University
West Lafayette, IN 47907 (USA)

Supporting Information for this article can be found under http://dx.doi.org/10.1002/ fin.201600511.

issues, the environmental sensitivity of MoS_2 may be exploited. Several recent studies reported that the surface functionalization of MoS_2 can drastically modulate the optoelectronic, electrochemical, and catalytic properties.[9c, 11] For example, molecular oxygen or p-type doping chemicals (e.g., 2,3,5,6-tetrafluoro-7,7,8,8-tetracyanoquinodimethane or F4TCNQ) can withdraw electrons from n-type semiconducting MoS_2. This can lead to suppression of nonradiative recombination and, therefore, a drastic enhancement in the PL emission quantum yield.[10-b, 11a, 12] Thus, the MoS_2 surface could be engineered to improve its physical properties to promote charge separation and transfer. Conversely, the environmental sensitivity of MoS_2 nanolayers requires surface protection and treatments, which may otherwise result in unwanted or poor performance when the materials are integrated into devices.

Herein, we demonstrate interfacial molecular engineering of large-area 2D MoS_2 films to enhance their photoelectrochemical properties (see Figure 1a). This study aims to develop a facile method for engineering MoS_2 nanolayers with porphyrin molecules to improve light-harvesting characteristics and to elucidate the underlying mechanisms. In particular, eight molecules from three porphyrin families were examined: zinc(II)-, iron(III)-, gallium(III)-centered, and metal-free protoporphyrin IX (ZnPP, FePP, GaPP, H_2PP); metal-free and zinc(II)-centered tetra(*N*-methyl-4-pyridyl)porphines (H_2T4, ZnT4); and metal-free and zinc(II)-centered tetraphenylporphyrins (H_2TPP, ZnTPP). These porphyrin molecules were physically adsorbed onto large-area ($\approx$1 cm^2) 2D MoS_2 films that had an average thickness of 2.8 nm. The functionalized MoS_2 films were then examined by using atomic force microscopy (AFM), micro-Raman spectroscopy, and photoelectrochemistry.

We observed that the currents generated under light illumination closely follow the absorption signature of MoS_2, which indicated that the photocurrent originates from thin layers of MoS_2 and that the current is an order of magnitude greater than in the bulk phase. We found that the photocurrent is greatly dependent upon the porphyrin molecules at the interface. For example, ZnPP demonstrated a maximum tenfold increase in photocurrent, whereas H_2T4 and ZnTPP do not alter the MoS_2 photocurrent significantly. We conclude that the photocurrent enhancements are closely correlated with the highest occupied molecular orbital (HOMO) levels of the interfacial porphyrin molecules. Higher photocurrent enhancements were observed for MoS_2 films functionalized with porphyrins with a higher HOMO level. The photocurrent can be further engineered by varying the bias voltage such that positive (negative) bias voltage enhances (suppresses) the photocurrent. These findings could form the basis for atomically thin MoS_2 for PEC conversion.

Experimental Section

Materials and Processing Procedures

Crystalline MoS_2 powder (0.3 g, Alfa Aesar) was placed into a three-neck flask before sealing and purging with nitrogen. Butyllithium solution (1.6 M) in hexane (3 mL, Sigma–Aldrich) was then injected into the flask by using a syringe pre-wetted with hexane. The intercalation of lithium ions into MoS_2 was achieved after 48 h. With positive nitrogen pressure, a second three-neck flask with a glass frit was connected to the previous flask. The glass frit had a medium pore size of 10–15 μm, which should filter all Li_xMoS_2 flakes. The flakes were collected onto the frit from the solvent by flipping the entire setup. A positive nitrogen pressure was applied to the first flask with the second flask kept under vacuum, so that all liquid passed through and left the Li_xMoS_2 on the frit. To remove excess butyllithium, the Li_xMoS_2 was washed with dry hexane (60 mL). Exfoliation was achieved by immersing the Li_xMoS_2 in water and applying tip-sonication at 5 W for 1 h, which resulted in a dark black mixture. The Li_xMoS_2 was exfoliated into single- and

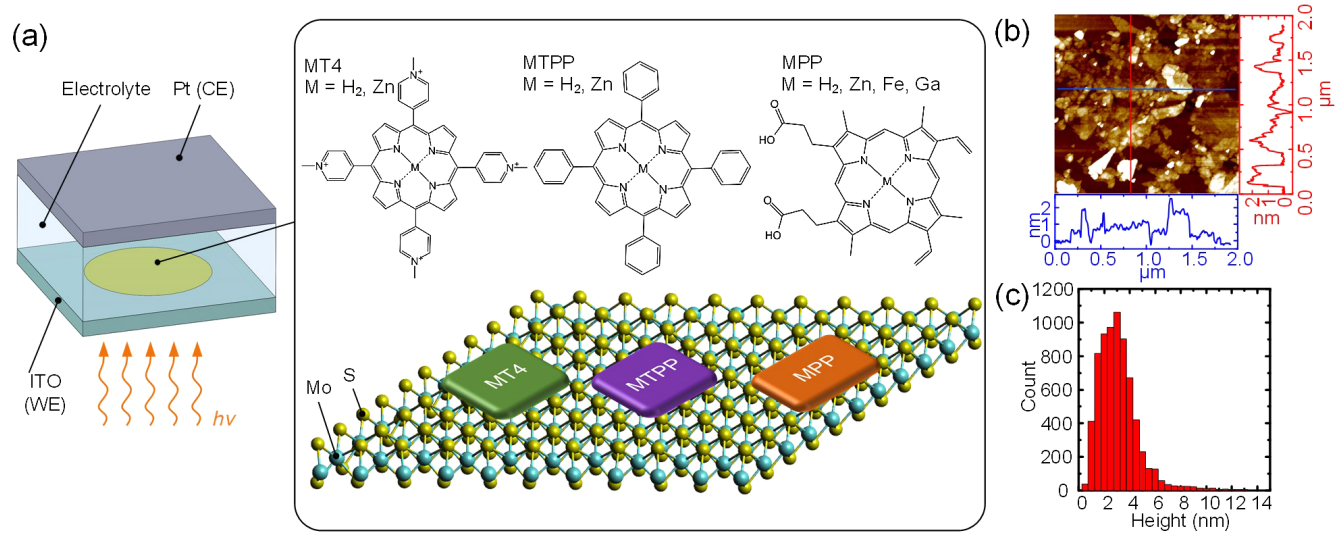

Figure 1. a) Schematic of a MoS_2-based photoelectrochemical cell. Chemically exfoliated solution-processed MoS_2 flakes were deposited on the ITO substrate and used as the working electrode (WE), with Pt used as the counter electrode (CE); 10 mM ascorbate was used as the electrolyte. Eight molecules from three porphyrin families were examined for their ability to improve the light-harvesting properties of MoS_2 in this study: MT4 (tetra(*N*-methyl-4-pyridyl)porphines; M = H_2 and Zn^{II}), MTPP (tetraphenylporphyrins; M = H_2 and Zn^{II}), and MPP (protoporphyrin IX; M = H_2, Zn^{II}, Fe^{III}, and Ga^{III}). b) Representative AFM image of a MoS_2 film deposited on a silicon wafer and height profiles along the lines of corresponding colors. c) Histogram of the film thickness measured from three random areas of three different MoS_2 samples, which indicates that the average thickness of the MoS_2 films is $\approx$2.8 nm.

few-layers by forced hydration generated by the Li ions interacting with water. The mixture was centrifuged at 5000 rpm for 20 min to remove unexfoliated materials. A stable colloidal green-black suspension was obtained at a concentration of ≈0.3 mg mL^{-1}. The nitrogen-purged solution can be stored in a refrigerator for months.

The deposition of thin MoS_2 films was carried out by using a vacuum filtration process. This process involved the filtration of suspended MoS_2 solution through a polycarbonate membrane (Fisher Scientific) with a pore size of 50 nm. The low-strength vacuum was created by using a water aspirator.[13] The exfoliated MoS_2 solution was diluted in deionized water (≈0.03 mg mL^{-1}) to help achieve uniform deposition. The liquid passed through the pores and MoS_2 flakes were collected on the membrane surface. As the flakes gathered around a pore, the flow rate decreased at that region and accelerated in uncovered area. This process was self-regulating and provided a uniformly deposited MoS_2 film with a controlled thickness by varying the amount of MoS_2 flakes in the suspension.[14] To transfer the film onto an ITO glass with ≈70–100 Ω□$^{-1}$ or a silicon wafer with a 100 nm oxidation layer, the MoS_2 film on the filter membrane was placed on the substrates, with the MoS_2 film placed against the substrate. By wetting the membrane with water, potential air bubbles could be driven away, which provided better contact between the film and the substrate. The polycarbonate membrane was then completely dissolved in chloroform, which left the MoS_2 film attached to the substrate (ITO glass or silicon wafer) by van der Waals interactions. The deposited films had a diameter of ≈1.3 cm. The MoS_2 films were annealed at 280 °C under argon for 1 h before functionalization with porphyrin molecules. Figure 1b shows an AFM image of a deposited MoS_2 film along with two typical height profiles. In Figure 1c, a statistical distribution of the deposited film thickness, collected from three random areas of three films, indicates that the overall average film thickness is ≈2.8 nm or 5–6 layers of MoS_2 flakes over an area of ≈1 cm^2.

Porphyrin Functionalization

ZnPP, FePP, GaPP, and H_2PP powders (Frontier Scientific) were solubilized in dimethyl sulfoxide (DMSO), whereas ZnT4 and H_2T4 (Frontier Scientific) were dissolved in deionized water for functionalization. The solvent for ZnTPP and H_2TPP (Sigma–Aldrich) was chloroform. To allow the porphyrins to adsorb physically onto the MoS_2 nanolayers, the MoS_2 films were immersed in 10 μM porphyrin solutions for 15 min, followed by rinsing with the respective solvents to remove unbound and weakly bound porphyrins.

Characterization and Instrumentation

A Perkin–Elmer Lambda 950 UV/Vis/near-IR spectrophotometer was used to record the absorption spectra of the MoS_2 films deposited on ITO/glass slides. The film samples used for PL, Raman, and AFM measurements were deposited onto silicon wafers. PL and Raman spectra were recorded under ambient conditions by using an inVia Renishaw confocal Raman microscope with laser excitation at λ = 633 nm.

Photoelectrochemical measurements were carried out by using a Princeton 263A galvanostat with a 150 W Xenon lamp. A long-pass filter (>400 nm, Thorlabs) and a short-pass filter (<710 nm, Thorlabs) were used to maintain the irradiation in the entire visible range at 110 mW over the entire film area. A PEC cell was custom-built with the MoS_2-deposited ITO as the working electrode and a platinum-coated glass as the counter electrode. The reference electrode was short-circuited with the counter electrode. For bias-voltage experiments, a solid silver wire was used as the reference electrode. For the spectrally resolved photocurrent measurements, the MoS_2 films were irradiated by using the same lamp equipped with an Oriel 1/8 m monochromator and a 360 nm blaze grating. The electrolyte in all our PEC measurements was 10 mM ascorbate in deionized water (pH 3).

2. Results and Discussion

2.1. Chemically Exfoliated Solution-Processed MoS_2 Nanolayers

Lithium ion intercalation assisted exfoliation of the MoS_2 crystal powder can produce single- and few-layer flakes with a typical size of several hundred nanometers. After a filtration-based deposition to form films 1 cm in diameter, chemically exfoliated MoS_2 flakes remained in their 1T metallic phase.[7] As a result, no distinct excitonic features were observed for the MoS_2 films, as shown in the absorption spectrum in Figure 2a.[7] High-temperature thermal annealing (280 °C) is critical

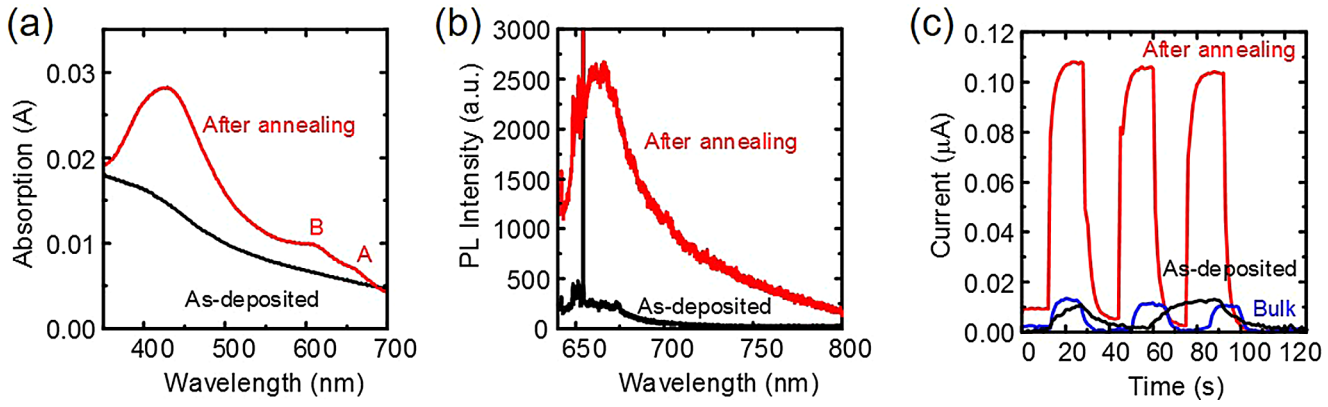

Figure 2. a) Absorption and b) PL spectra of as-deposited (1T phase) and annealed (2H phase) MoS_2 films. A HeNe laser at λ = 633 nm was used for emission measurements. c) Photocurrents generated from a chemically exfoliated solution-processed MoS_2 film before (black) and after (red) thermal annealing. An untreated MoS_2 powder film (bulk phase) was also examined as a control (blue). Visible light (λ = 400–710 nm) was used for photocurrent measurements and 10 mM ascorbate in deionized water was used as the electrolyte.

in film preparation because it converts MoS_2 flakes from the 1T metallic phase to a 2H semiconductor. After annealing, two distinct band structures emerged in the absorption spectrum, which were assigned as A and B interband excitonic transitions at the K point of Brillouin zone.[15] The A and B features are at approximately $\lambda = 660$ (1.88 eV) and 612 nm (2.03 eV), whereas the most dominant absorption appears at $\lambda \approx 430$ nm.[1a,16]

Figure 2b shows the effect of thermal annealing on the PL spectra of the MoS_2 film. PL emission is barely observed before annealing because of the metallic crystal structure in the 1T phase. The high-temperature annealing not only restores the 2H phase from the 1T phase but also reduces crystal defects, which results in significant PL enhancement.[7] Due to the chosen excitation wavelength at $\lambda = 633$ nm, we observed the transition of exciton A only from the thin MoS_2 film at approximately $\lambda = 660$ nm.[1b] The sharp peak at $\lambda \approx 654$ nm is the Raman signature of the silicon wafer ($\approx 520\ cm^{-1}$), whereas the less prominent features from $\lambda = 648$ to 650 nm are the Raman modes of MoS_2 (from 380 to 405 cm^{-1}).[17]

Photocurrent measurements of a MoS_2 film before and after thermal annealing, along with bulk MoS_2, are shown in Figure 2c. The MoS_2 films before and after annealing were prepared from the chemically exfoliated MoS_2 flake solution, whereas the bulk MoS_2 sample was deposited onto the ITO from briefly sonicated MoS_2 powder (i.e. no Li-intercalation-based exfoliation process). Thus, the bulk MoS_2 sample should have retained its semiconducting properties with an indirect bandgap. Positive short-circuit currents were observed for all MoS_2 films under visible-light illumination ($\lambda = 400$–710 nm), in which the electrons were collected at the working electrode (i.e. MoS_2-deposited ITO anode). The holes, created by electron injection from MoS_2 to the ITO, were reduced by oxidation of the electrolyte:

$$\text{ascorbate} \rightarrow \text{dehydroascorbate} + 2e^- + 2H^+ \quad (1)$$

The oxidized electrolyte (dehydroascorbate) diffuses to the counter electrode (Pt cathode) and becomes reduced to its initial form. As shown in Figure 2c, the annealed MoS_2 film demonstrates a clear response to light irradiation and a maximum photocurrent of approximately 0.12 μA was observed. Under identical conditions, bulk MoS_2 exhibited photocurrent responses that were an order of magnitude weaker at approximately 0.01 μA, whereas as-deposited thin MoS_2 film in metallic 1T phase did not generate stable photocurrents, as anticipated.[1b,4c,18]

2.2. Porphyrin-Functionalized MoS_2 Films

MoS_2 thin films were functionalized with porphyrin molecules and their properties were compared with those of pristine MoS_2 films. Figure 3a shows the absorption spectra of the MoS_2 film before and after ZnT4 adsorption. The porphyrin-functionalized MoS_2 mostly follows the absorption features of the pristine film, but a minor change is observed at approximately $\lambda = 450$ nm, which corresponds to the Soret band (singlet-state transition from S_0 to S_2) of ZnT4.[19] Porphyrin molecules have strong optical absorption in the Soret (typically $\lambda =$ 400–450 nm) and Q ($S_0 \rightarrow S_1$; $\lambda = 550$–650 nm) bands due to their electron-rich π systems, and the transition energies depend strongly on the presence and type of core metal ions (Figure S1 in the Supporting Information).[20] The weak Soret and Q-band signatures, compared with MoS_2 absorption, suggest that the amount of adsorbed porphyrins is minimal.

To examine the porphyrin adsorption further, we raster-scanned PL spectra from an area of the MoS_2 film (20×20 μm) before and after ZnT4 functionalization by using $\lambda = 633$ nm excitation. The PL emission at $\lambda = 660$ nm was used to reconstruct a 2D image of the pristine MoS_2 film (Figure 3b, left), which exhibited near-uniform emission properties. Compared with the pristine film, there was a drastic PL enhancement across the entire area after ZnT4 functionalization (Figure 3b, right). Here, the PL measurements were performed on exactly the same spot before and after porphyrin adsorption, and both the 2D PL maps were reconstructed on the same intensity scale. To verify the porphyrin functionalization further, only

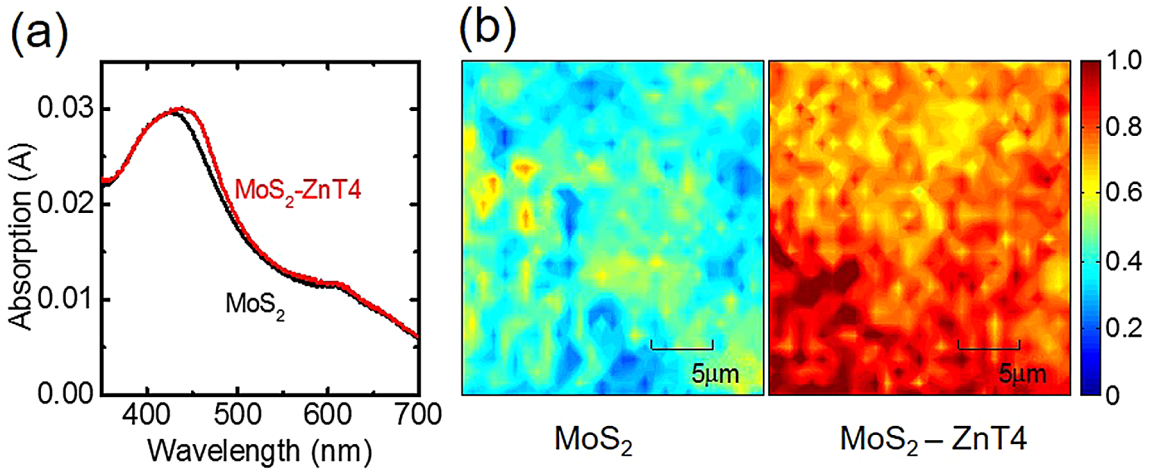

Figure 3. a) Absorption spectra of the MoS_2 film before and after ZnT4 functionalization. b) Raster-scanned 2D PL map of the same area of a MoS_2 film before (left) and after (right) ZnT4 functionalization. The sample was excited at $\lambda = 633$ nm, and the PL maps are reconstructed based on the PL emission at $\lambda = 660$ nm. The significant PL intensity increase indicates the adsorption of porphyrin molecules on the MoS_2 film.

part of the film was immersed in a porphyrin solution, and a PL map was recorded that spanned both pristine and functionalized domains (Figure S8). A stark difference in PL intensity was observed between the pristine and functionalized regions, which confirmed the porphyrin adsorption. Porphyrin molecules, including ZnT4, exhibit strong emission properties after photoexcitation; they emit fluorescence through singlet-state transitions ($S_1 \rightarrow S_0$) or phosphorescence after intersystem crossing ($T \rightarrow S_0$) or both.[20a] Porphyrins such as FePP do not display strong emission due to efficient nonradiative decay through the d orbital of the core metal ion.[21] ZnT4 shows strong fluorescence emission from $\lambda = 600$ to 700 nm after excitation (Figure S1).[22] Therefore, the PL intensity increase shown in Figure 3b is attributed to the ZnT4 porphyrins, and indicates their adsorption on the MoS_2 film. From the absorption and PL emission results in Figure 3, we concluded that MoS_2 films are functionalized with porphyrins.

To elucidate the nature of the MoS_2–porphyrin interaction, we examined the Raman spectra of MoS_2 nanolayers before and after porphyrin functionalization (in this case, FePP). We found that there were no significant changes in the MoS_2 signatures (A_{1g} and E^1_{2g}) before and after functionalization with the porphyrins. This observation suggests that porphyrin molecules do not form chemical bonds with 2D MoS_2; rather, they interact with MoS_2 through physisorption. Additionally, a recent study revealed that organometallic compounds adsorbed on TMDC nanolayers demonstrate consistent X-ray photoelectron spectroscopy (XPS) features regardless of the adsorption.[11b] Our results strongly suggest that metalloporphyrins physically adsorb on the MoS_2 nanolayers instead of forming chemical bonds.

Absorption spectra and 2D PL maps were also recorded with ZnPP, FePP, and ZnTPP (Figures S2–4), which together clearly show the adsorption of the porphyrins on MoS_2 films. For the MoS_2 films with and without ZnPP (Figure S2a) and FePP (Figure S3a), no apparent changes were observed in the absorption spectra, whereas ZnPP PL emission was evident on the MoS_2. Although FePP on MoS_2 does not display any PL signature due to its nonradiative decay mechanism, the film shows a strong photocurrent enhancement (see below). Given the similar molecular structures, ZnPP and FePP should have comparable surface coverage on MoS_2. Compared with ZnPP and FePP, the signatures of the adsorbed ZnTPP molecules appear to be more prominent in both the absorption spectrum and the PL map (Figure S4). Additionally, we measured the 2D PL map of the as-deposited MoS_2 functionalized with ZnPP. Given that the unannealed MoS_2 sample is non-emissive due to its metallic 1T phase (Figure 2b), the PL emission clearly shows the attachment of ZnPP (Figure S5).

The effects of porphyrin functionalization on the photocurrents are presented in Figure 4. Figure 4a shows that the photocurrent of the MoS_2 film functionalized with ZnPP increases by nearly an order of magnitude from 0.14 to 1.1 μA, compared with the pristine film, under visible-light illumination. The photocurrent of the MoS_2-ZnPP was also measured as a function of irradiation intensity, and demonstrated a monotonic increase with increasing intensity, as expected (Figure S9). To elucidate the origin of the photocurrent enhancement, the corresponding action spectra were collected, and are shown in Figure 4b. Here, the photocurrents of pristine MoS_2 and MoS_2-ZnPP films were measured from $\lambda = 350$ to 800 nm with increments of 25 nm, which were then compared with the absorption spectrum of a pristine MoS_2 film. It should be noted that the MoS_2 film in the photocurrent action spectra measurement was thicker than other MoS_2 samples; because the light power after the monochromator was significantly lower at each wave-

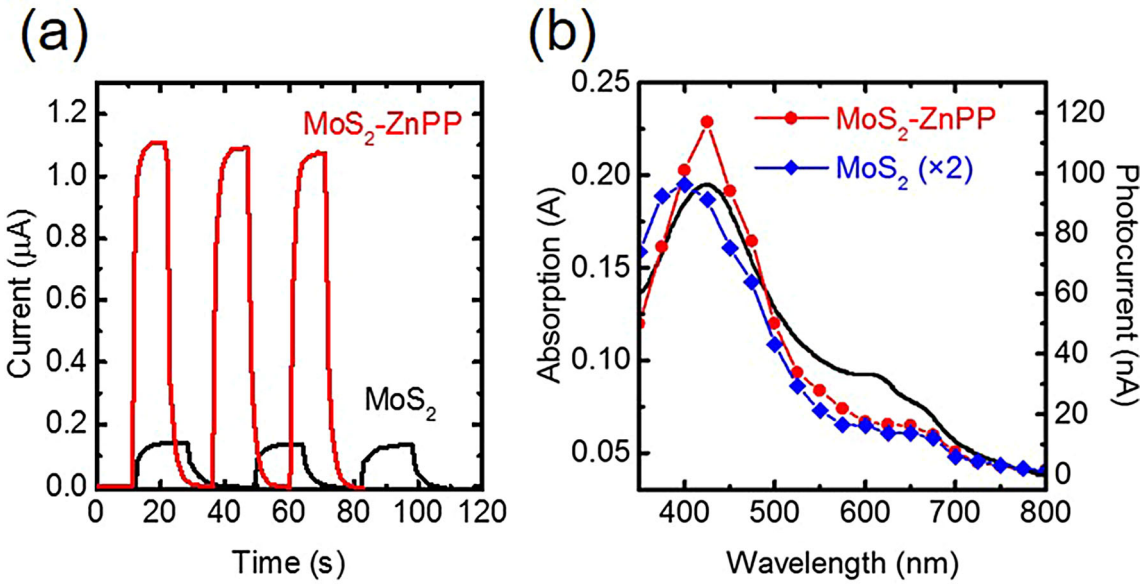

Figure 4. a) Photoelectrochemical measurement of the MoS_2 film deposited on an ITO substrate before and after functionalization of ZnPP molecules. The MoS_2 film demonstrates nearly an order of magnitude greater photocurrents after ZnPP adsorption. b) Photocurrents of the MoS_2 film before (blue) and after (red) ZnPP adsorption as a function of excitation wavelength. The optical absorption spectrum of pristine MoS_2 film is also shown in black. Note that the photocurrent of the MoS_2-ZnPP film is ten times greater than the pristine film.

length, a greater amount of MoS_2 flakes was used to obtain sufficient photocurrent. The photocurrents of both MoS_2 and MoS_2-ZnPP films generally follow the absorption spectrum. Notably, the photocurrent of MoS_2-ZnPP at each measured wavelength is two times greater than that of the pristine film. This observation indicates that the adsorbed porphyrin molecules facilitate charge separation after photoexcitation and suppress recombination in MoS_2, which thus enhances photocurrent generation throughout the visible range. From the photocurrent of the MoS_2-ZnPP film, we estimate that the incident photon-to-current efficiency (IPCE) at $\lambda = 425$ nm is approximately 1%.

A closer examination revealed several important details in the action spectra. Although the photocurrent from $\lambda = 550$ to 700 nm generally follows the A and B excitonic features, the photocurrent is not as prominent as the absorption. In comparison, the photocurrent from $\lambda = 350$ to 500 nm matches the C exciton feature closely, which suggests that the charge separation and recombination suppression in the MoS_2 film by interfacial porphyrins are more efficient in high-energy excitons. Another interesting feature is the small, yet distinct, absorption peak at approximately $\lambda = 425$ nm that corresponds to the Soret band of ZnPP. The sharp increase in photocurrent at the Soret band may result from the charge-transfer process from the photoexcited ZnPP to the conduction band of MoS_2. These results indicate that the adsorbed porphyrins could contribute as photosensitizers although their contributions to the entire photocurrent are very modest. The majority of the photocurrent originating from MoS_2 and porphyrins helps separate the photogenerated charge and collect photocurrent. Otherwise, the photocurrent would mostly follow the absorption features of the porphyrins rather than MoS_2, which was observed previously with porphyrin–carbon nanotube hybrids.[20a] Finally, the relative amount of MoS_2 flakes (i.e. thickness of the film) and adsorbed porphyrins is critical in determining photocurrent outputs, as seen in Figure 4. Given that porphyrins adsorb on the MoS_2 surface, the degree of photocurrent increase would not be strongly dependent upon the thickness of MoS_2 films. The thin MoS_2-ZnPP film ($\approx$1.8 μg of MoS_2 flakes) generated a nearly tenfold increase compared with pristine MoS_2 (Figure 4a), whereas the thick film ($\approx$18 μg of MoS_2 flakes) produced a twofold enhancement (Figure 4b). In a thicker film, the separated charges have a greater probability of recombination before reaching the ITO electrode.

2.3. Interfacial Charge-Transfer Mechanism

In addition to ZnPP, seven other porphyrin species (H_2T4, ZnT4, ZnTPP, H_2TPP, GaPP, H_2PP, and FePP; see Figure 1 for molecular structures) were explored for their ability to enhance the photocurrent of MoS_2 under identical experimental conditions. Here we define the photocurrent enhancement, or $(I-I_o)/I_o$, as the change in photocurrent after porphyrin functionalization over the initial photocurrent of pristine MoS_2 film (I_o). This photocurrent enhancement is presented as a function of the HOMO level of each porphyrin species in Figure 5a.[23] All the detailed photocurrent measurements can be found in Figure S6. The porphyrin species show a wide range of enhancement activities. Although ZnPP demonstrates an increase of nearly an order of magnitude, there were no significant changes in the measured photocurrent after adsorption of H_2T4 and ZnTPP. Both ZnT4 and H_2TPP exhibited an approximately 100% enhancement in the photocurrent (i.e. a twofold increase in photocurrent). The MoS_2 films functionalized with GaPP and H_2PP showed almost the same photocurrent enhancement, whereas FePP and ZnPP improved the photocurrent generation in MoS_2 films by approximately 500 and 800%, respectively. The lack of enhancement with H_2T4 and ZnTPP is not due to the inefficiency of porphyrin functionalization, as discussed earlier. A porphyrin emission was observed for all

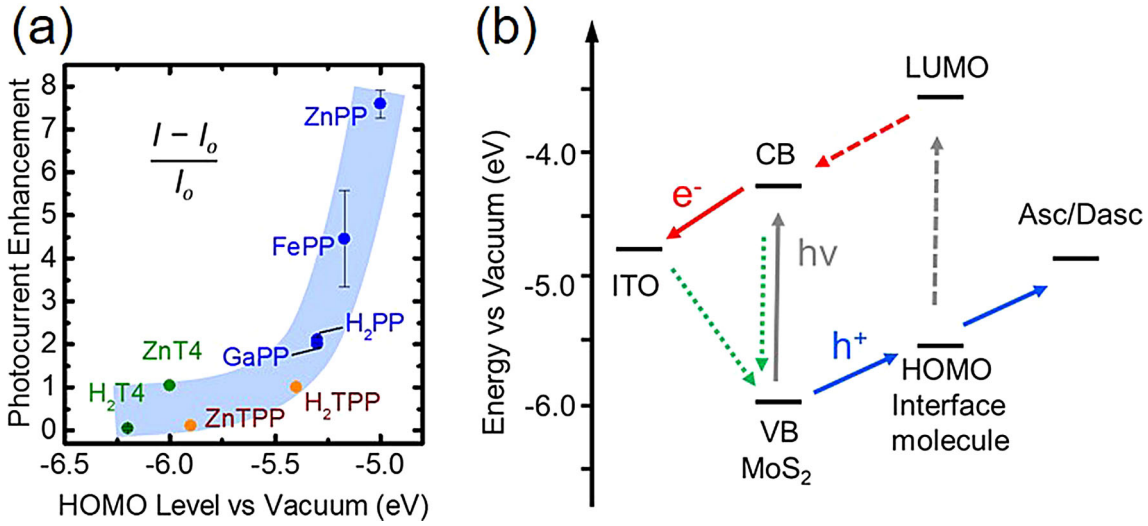

Figure 5. a) Photocurrent enhancement of MoS_2 films functionalized with various porphyrin species. The photocurrent enhancement or $(I-I_o)/I_o$ is defined as the change in photocurrent before and after porphyrin adsorption over the initial photocurrent of pristine MoS_2. The photocurrent enhancement is strongly correlated with the HOMO level of the porphyrin. The blue shading is a guide for the eye. b) Proposed mechanism of photocurrent enhancement in MoS_2 films after engineering an interface with porphyrin species. Red and blue arrows indicate electron injection and hole transfer, respectively. Grey lines show light illumination, and green arrows represent possible charge-recombination pathways.

samples except for MoS_2-FePP because FePP is nonemissive. Additionally, porphyrins from the same family, such as GaPP, H_2PP, FePP, and ZnPP, should have similar adsorption properties, yet they show drastic differences in photocurrent enhancement.

The three porphyrin families (T4, TPP, and PP) may be considered in understanding photocurrent enhancement behavior. Both H_2T4 and ZnT4 have a pyridium substituent group, which provides positive charge in aqueous electrolyte solutions. For H_2TPP and ZnTPP, a net neutral charge is expected given their phenyl ligand.[24] The carboxylic moieties of ZnPP, FePP, GaPP, and H_2PP render them negatively charged in the aqueous phase. Although both T4 and TPP families show relatively small enhancement behavior compared with the PP family, the ligand groups of the three families do not consistently match the photocurrent enhancements. Additionally, the metal cations at the porphyrin cores are not correlated with the photocurrent activities; for example, there is no enhancement with ZnTPP, whereas ZnPP shows a drastic increase.

We found that the photocurrent enhancement is strongly associated with the HOMO levels of the porphyrin species, as shown in Figure 5a. The enhancement factor increases exponentially as a function of the HOMO level of the porphyrin (Figure S7):

$$\frac{I - I_0}{I_0} = 0.22 + 0.14\, e^{\frac{HOMO - VBM}{0.23}} \quad (2)$$

in which I and I_0 represent the photocurrents of the porphyrin-functionalized and pristine MoS_2, respectively, and VBM is the valence band maximum of MoS_2. From the strong correlation of the photocurrent enhancement with the HOMO level (Figure 5a), we propose a mechanism for the interfacial charge-transfer process in the MoS_2–porphyrin hybrid system, as illustrated in Figure 5b. Upon photoabsorption, electrons in the pristine MoS_2 film are excited into the conduction band (CB) and may then be injected into the ITO working electrode. As the transferred electrons are collected at the ITO, the work function of which is placed approximately 0.45 eV lower than the conduction band minimum (CBM) of MoS_2,[25] the holes left in MoS_2 can be reduced by an electrolyte reaction with a redox potential that is positioned significantly higher than the VBM of MoS_2.[26] The oxidized dehydroascorbate molecules diffuse to the counter electrode and become reduced to ascorbate, which completes the electrical circuit. In addition to the photocurrent generation mechanism, there are also several processes that can compete with the interfacial charge transfer. First, the photoexcited electrons in the CB of MoS_2 may relax nonradiatively and return to the VB. There could also be back-transfer of electrons from the ITO to the MoS_2 film. These processes facilitate the recombination of photoinduced charges, which thus reduces the photocurrent.

The charge-recombination processes may be suppressed by porphyrins adsorbed on the MoS_2 films, which would thus enhance the photocurrent. With porphyrins for which the HOMO level is positioned higher than the VBM of MoS_2, the holes created after photoexcitation can be readily transferred to the interfacial porphyrins, which suppresses recombination and/or back reaction. The suppression mechanism with interfacial porphyrins should be far more effective compared with pristine MoS_2 films that rely solely on the slow diffusion of the electrolyte in solution. The oxidized porphyrins are reduced by the ascorbate→dehydroascorbate reaction. In this mechanism, the charge separation and transfer should be more efficient with porphyrins with higher HOMO levels, such as ZnPP and FePP, which give greater photocurrent enhancements. In contrast, a photocurrent enhancement is not expected with porphyrins for which the HOMO levels are close to or lower than the VBM of MoS_2. From an energetics perspective, the hole transfer from MoS_2 to H_2T4 and ZnTPP is minimal or unlikely. Indeed, a negligible improvement was confirmed experimentally. It should be noted that the CBM and VBM potentials shown in Figure 5b are for monolayer MoS_2, which may be slightly different from the values for few-layers MoS_2, given the layer-number-dependent properties of MoS_2.[27]

In addition to the porphyrins examined, other molecules may also be used to improve photocurrent in MoS_2. We explored other porphyrins (CuT4) and phthalocyanines (nickel tetrasulfonated phthalocyanine), which demonstrated a wide range of photocurrent activities (Figure S6). However, the results are not included here because their HOMO/LUMO levels are not known, to the best of our knowledge. We also note that there is a minor source of photocurrent depending on the molecules used. A class of porphyrins (e.g., ZnPP in Figure 4b) can contribute to the current as a photosensitizer, by injecting electrons into MoS_2 that can then be shuffled and collected at the electrode.

2.4. Effect of Bias Voltage

Last, we examined the effects of bias voltage on photocurrent measurements of MoS_2 and MoS_2-ZnPP films (Figure 6). Here, a voltage range from −200 to 200 mV against the Ag reference electrode was applied. As seen in Figure 6a and c, the photocurrent responses of pristine MoS_2 at zero bias voltage (short-circuit current) are nearly identical to those shown in Figure 2c and Figure 4a. Once a positive voltage is applied, the photocurrent and dark currents (i.e. baseline) both experience increases. For example, the photocurrent and dark current increase from approximately 110 to 200 nA and from approximately 0 to 450 nA at 50 mV, respectively. Both currents gradually increase with increasing bias voltage. At 200 mV, the photocurrent from the pristine MoS_2 film reached approximately 300 nA, which is about three times greater than with no bias voltage. Negative bias voltages, however, reversed this trend. At −50 mV, photocurrents were barely observed, whereas the dark current became negative at approximately −300 nA. An increase in negative bias voltage leads to negative photocurrent, which implies that photogenerated electrons are collected at the counter electrode instead of the working electrode. After a further increase in negative bias voltage, the negative photocurrent escalated, to about −250 nA at −200 mV.

The MoS_2 film functionalized with ZnPP shows behavior that is generally similar to pristine MoS_2 under various bias voltag-

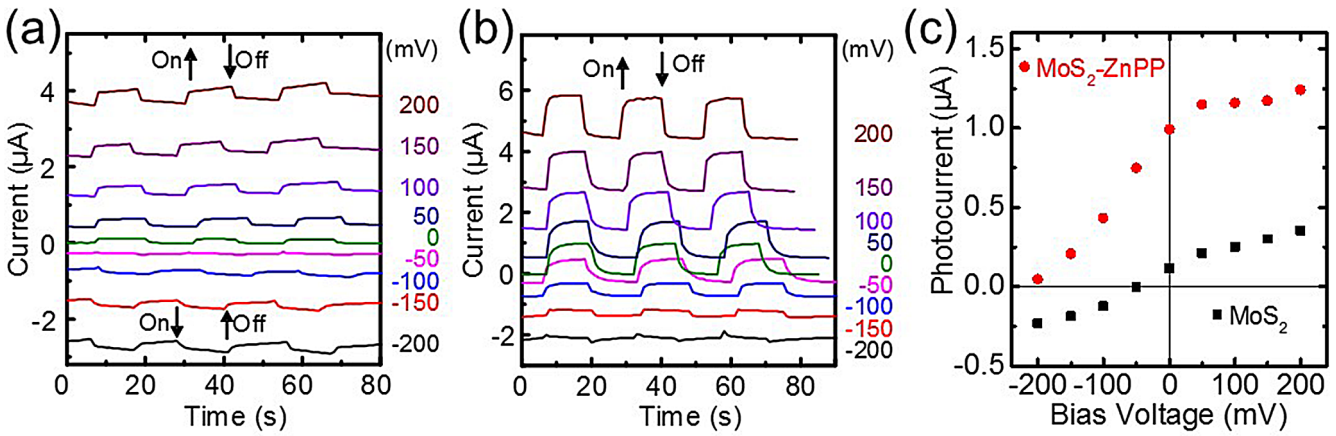

Figure 6. a) Currents of a) pristine MoS_2 and b) MoS_2-ZnPP films as a function of externally applied bias voltage under light illumination. c) Photocurrent responses of MoS_2 (■) and MoS_2-ZnPP (●) films as a function of bias voltage; a solid silver wire was used as the reference electrode.

es, as shown in Figure 6b and c. At 50 mV, the ZnPP-MoS_2 film experienced a photocurrent enhancement from approximately 1 to 1.2 μA, whereas the dark current also increased from approximately 0 to 0.55 μA. Both the photocurrent and the dark current continued to increase, reaching approximately 1.4 and 4.5 μA, respectively, at 200 mV. Similar to pristine MoS_2, the photocurrent gradually decreased with increasing negative bias voltage from 1 μA at 0 mV to zero at −200 mV. Negative photocurrent would be observed at more-negative bias voltages.

The effects of bias voltage can be understood within our proposed mechanism. With a positive bias voltage, the work function of the ITO may be shifted downward against the vacuum, away from the CBM of MoS_2. As a result, the electron flow from MoS_2 or MoS_2–porphyrin films to the ITO becomes more favorable due to a larger driving potential and reduced recombination within the system, which results in increased photocurrent. In contrast, negative voltages raise the ITO work function and thus the difference between the ITO and the CBM of MoS_2 is decreased, which reduces the driving potential for electron flow into the ITO. A further increase in negative bias voltage can place the ITO work function above the CBM of MoS_2, which changes the direction of electron flow (i.e. negative photocurrent). The negative photocurrents grow with higher ITO work function at greater negative bias voltages. The adsorbed porphyrin molecules make a significant impact not only on the photocurrent magnitude but also on the reversal of the photocurrent direction. The inflection point changes from approximately −50 mV with pristine MoS_2 to roughly −200 mV with the MoS_2-ZnPP sample, as shown in Figure 6c. Thus, ZnPP is responsible for the difference in the inflection points (≈150 mV), which is less than the gap (≈500 mV) between the ITO work function and the CBM of MoS_2. This discrepancy may be understood by considering that our MoS_2 thin films are few-layers thick, unlike the CBM and VBM of monolayers shown in Figure 5b, and thus the actual gap should be smaller. Overall, these results confirm the effective modulation of MoS_2 properties by interfacial porphyrins.

3. Conclusion

We have successfully fabricated large-area 2D MoS_2 films from chemically exfoliated flakes and studied their optical and photoelectrochemical properties. Eight porphyrin species from three distinct families were examined for their ability to modulate the photoelectrochemical properties of MoS_2 films. We observed a maximum tenfold increase in photocurrent from the porphyrin-functionalized MoS_2 compared with pristine MoS_2. The photocurrent enhancements correlate to the HOMO energies of the porphyrins. The higher the energy of the HOMO, the greater the photocurrent enhancement produced by the functionalized MoS_2 films. The interfacial porphyrins significantly suppress charge recombination pathways and enhance the photocurrent. We also demonstrate that adsorbed porphyrins significantly modulate both the magnitude of the photocurrent and the direction of electron flow. Our results are critical to understanding the fundamental properties of MoS_2 interfaced with porphyrins or other organic compounds in the context of using TMDCs as light-harvesting materials.

Acknowledgements

This work was financially supported by the US National Science Foundation.

Keywords: light harvesting · molybdenum disulfide · nanolayers · photocurrent · porphyrins

[1] a) K. F. Mak, C. Lee, J. Hone, J. Shan, T. F. Heinz, *Phys. Rev. Lett.* **2010**, *105*, 136805; b) A. Splendiani, L. Sun, Y. Zhang, T. Li, J. Kim, C.-Y. Chim, G. Galli, F. Wang, *Nano Lett.* **2010**, *10*, 1271.

[2] a) J. Pu, Y. Yomogida, K.-K. Liu, L.-J. Li, Y. Iwasa, T. Takenobu, *Nano Lett.* **2012**, *12*, 4013; b) Y. Yoon, K. Ganapathi, S. Salahuddin, *Nano Lett.* **2011**, *11*, 3768; c) Y. Deng, Z. Luo, N. J. Conrad, H. Liu, Y. Gong, S. Najmaei, P. M. Ajayan, J. Lou, X. Xu, P. D. Ye, *ACS Nano* **2014**, *8*, 8292.

[3] a) D. Lembke, A. Kis, *ACS Nano* **2012**, *6*, 10070; b) B. Radisavljevic, A. Radenovic, J. Brivio, V. Giacometti, A. Kis, *Nat. Nanotechnol.* **2011**, *6*, 147; c) M.-L. Tsai, S.-H. Su, J.-K. Chang, D.-S. Tsai, C.-H. Chen, C.-I. Wu, L.-J. Li, L.-J. Chen, J.-H. He, *ACS Nano* **2014**, *8*, 8317; d) Q. H. Wang, K. Kalantar-

Zadeh, A. Kis, J. N. Coleman, M. S. Strano, *Nat. Nanotechnol.* **2012**, *7*, 699.

[4] a) G. Kline, K. Kam, D. Canfield, B. Parkinson, *Solar Energy Materials* **1981**, *4*, 301; b) A. Laurie, D. J. Riley, *J. Mater. Chem. A* **2013**, *1*, 8935; c) K. G. Zhou, N. N. Mao, H. X. Wang, Y. Peng, H. L. Zhang, *Angew. Chem. Int. Ed.* **2011**, *50*, 10839; *Angew. Chem.* **2011**, *123*, 11031; d) M. Buscema, J. O. Island, D. J. Groenendijk, S. I. Blanter, G. A. Steele, H. S. van der Zant, A. Castellanos-Gomez, *Chem. Soc. Rev.* **2015**, *44*, 3691; e) J. Zhang, S. Najmaei, H. Lin, J. Lou, *Nanoscale* **2014**, *6*, 5279; f) C.-J. Liu, S.-Y. Tai, S.-W. Chou, Y.-C. Yu, K.-D. Chang, S. Wang, F. S.-S. Chien, J.-Y. Lin, T.-W. Lin, *J. Mater. Chem.* **2012**, *22*, 21057; g) S.-Y. Tai, C.-J. Liu, S.-W. Chou, F. S.-S. Chien, J.-Y. Lin, T.-W. Lin, *J. Mater. Chem.* **2012**, *22*, 24753; h) M. Wu, Y. Wang, X. Lin, N. Yu, L. Wang, L. Wang, A. Hagfeldt, T. Ma, *Phys. Chem. Chem. Phys.* **2011**, *13*, 19298; i) G. Djemal, N. Müller, U. Lachish, D. Cahen, *Solar Energy Materials* **1981**, *5*, 403.

[5] A. Goldberg, A. Beal, F. Levy, E. Davis, *Philos. Mag.* **1975**, *32*, 367.

[6] a) Y. Li, H. Wang, L. Xie, Y. Liang, G. Hong, H. Dai, *J. Am. Chem. Soc.* **2011**, *133*, 7296; b) H. Li, C. Tsai, A. L. Koh, L. Cai, A. W. Contryman, A. H. Fragapane, J. Zhao, H. S. Han, H. C. Manoharan, F. Abild-Pedersen, *Nat. Mater.* **2015**; c) Q. Xiang, J. Yu, M. Jaroniec, *J. Am. Chem. Soc.* **2012**, *134*, 6575.

[7] G. Eda, H. Yamaguchi, D. Voiry, T. Fujita, M. Chen, M. Chhowalla, *Nano Lett.* **2011**, *11*, 5111.

[8] M. Chhowalla, H. S. Shin, G. Eda, L.-J. Li, K. P. Loh, H. Zhang, *Nat. Chem.* **2013**, *5*, 263.

[9] a) X. Huang, Z. Zeng, H. Zhang, *Chem. Soc. Rev.* **2013**, *42*, 1934; b) G. R. Bhimanapati, Z. Lin, V. Meunier, Y. Jung, J. Cha, S. Das, D. Xiao, Y. Son, M. S. Strano, V. R. Cooper, *ACS Nano* **2015**, *9*, 11509; c) V. Nicolosi, M. Chhowalla, M. G. Kanatzidis, M. S. Strano, J. N. Coleman, *Science* **2013**, *340*, 1226419.

[10] a) H. Shi, R. Yan, S. Bertolazzi, J. Brivio, B. Gao, A. Kis, D. Jena, H. G. Xing, L. Huang, *ACS Nano* **2013**, *7*, 1072; b) H. Nan, Z. Wang, W. Wang, Z. Liang, Y. Lu, Q. Chen, D. He, P. Tan, F. Miao, X. Wang, *ACS Nano* **2014**, *8*, 5738.

[11] a) S. Tongay, J. Zhou, C. Ataca, J. Liu, J. S. Kang, T. S. Matthews, L. You, J. Li, J. C. Grossman, J. Wu, *Nano Lett.* **2013**, *13*, 2831; b) J. Choi, H. Zhang, J. H. Choi, *ACS Nano* **2016**, *10*, 1671.

[12] S. Mouri, Y. Miyauchi, K. Matsuda, *Nano Lett.* **2013**, *13*, 5944.

[13] H. Zhang, B. A. Baker, T. G. Cha, M. D. Sauffer, Y. Wu, N. Hinkson, M. A. Bork, C. M. McShane, K. S. Choi, D. R. McMillin, *Adv. Mater.* **2012**, *24*, 5447.

[14] G. Eda, G. Fanchini, M. Chhowalla, *Nat. Nanotechnol.* **2008**, *3*, 270.

[15] A. Beal, J. Knights, W. Liang, *J. Phys. D J. Phys. C: Solid State Phys.* **1972**, *5*, 3540.

[16] M. Ye, D. Winslow, D. Zhang, R. Pandey, Y. Yap, *Photonics* **2015**, *2*, 288.

[17] I. De Wolf, *Semicond. Sci. Technol.* **1996**, *11*, 139.

[18] A. Kuc, N. Zibouche, T. Heine, *Phys. Rev. B* **2011**, *83*, 245213.

[19] Z. Zhang, R. Hu, Z. Liu, *Langmuir* **2000**, *16*, 1158.

[20] a) H. Zhang, M. A. Bork, K. J. Riedy, D. R. McMillin, J. H. Choi, *J. Phys. Chem. C* **2014**, *118*, 11612; b) K. Kalyanasundaram, M. Neumann-Spallart, *J. Phys. Chem.* **1982**, *86*, 5163.

[21] H. Tajima, K. Shimatani, T. Komino, S. Ikeda, M. Matsuda, Y. Ando, H. Akiyama, *Colloids Surf. A* **2006**, *284*, 61.

[22] H. Wang, L. Yu, Y.-H. Lee, Y. Shi, A. Hsu, M. L. Chin, L.-J. Li, M. Dubey, J. Kong, T. Palacios, *Nano Lett.* **2012**, *12*, 4674.

[23] a) E. Moons, A. Goossens, T. Savenije, *J. Phys. Chem. B* **1997**, *101*, 8492; b) N. Tao, *Phys. Rev. Lett.* **1996**, *76*, 4066; c) K. Salazar-Salinas, L. A. Jauregui, C. Kubli-Garfias, J. M. Seminario, *J. Chem. Phys.* **2009**, *130*, 105101; d) T. Oku, T. Noma, A. Suzuki, K. Kikuchi, S. Kikuchi, *J. Phys. Chem. Solids* **2010**, *71*, 551; e) T. B. Pinter, E. L. Dodd, D. S. Bohle, M. J. Stillman, *Inorg. Chem.* **2012**, *51*, 3743; f) A. R. Bizzarri, S. Cannistraro, *Chem. Phys. Lett.* **2004**, *395*, 222.

[24] K. Kalyanasundaram, *Inorg. Chem.* **1984**, *23*, 2453.

[25] Y. Park, V. Choong, Y. Gao, B. Hsieh, C. Tang, *Appl. Phys. Lett.* **1996**, *68*, 2699.

[26] T. Iyanagi, I. Yamazaki, K. F. Anan, *Biochimica et Biophysica Acta, Bioenergetics* **1985**, *806*, 255.

[27] a) T. Cheiwchanchamnangij, W. R. Lambrecht, *Phys. Rev. B* **2012**, *85*, 205302; b) J. K. Ellis, M. J. Lucero, G. E. Scuseria, *Appl. Phys. Lett.* **2011**, *99*, 261908.

Manuscript received: May 17, 2016
Accepted Article published: June 15, 2016
Final Article published: ■■ ▮▮, 0000

ARTICLES

*H. Zhang, J. Choi, A. Ramani, D. Voiry, S. N. Natoli, M. Chhowalla, D. R. McMillin, J. H. Choi**

■■ – ■■

Engineering Chemically Exfoliated Large-Area Two-Dimensional MoS_2 Nanolayers with Porphyrins for Improved Light Harvesting

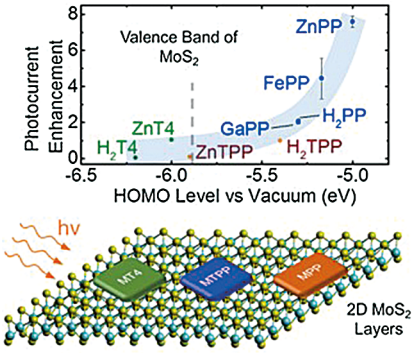

Layer by layer: Modulation of the photoelectrochemical properties of MoS_2 nanolayers is achieved by interfacial engineering with an array of porphyrin molecules. A maximum tenfold increase in photocurrent is observed for MoS_2 with Zn-centered protoporphyrins. A unique modulation of photoelectrochemical properties of 2D semiconductors and a fundamental understanding of photoinduced charge transfer for MoS_2-based light harvesting is presented.